

# DYNAMIC CHARACTERISTICS OF THE THRUST VECTORIZING CONTROL BY HIGHLY COMPRESSIBLE COANDA EFFECTS

**Yeol Lee\*, SangHoon Park\*, HongBeen Chang\*, YongHo Cho\*\***  
**\*Korea Aerospace University, South Korea**  
**\*\*Seyon Engineering & System Co., South Korea**

## Abstract

*Fluidic Thrust Vector Control (FTVC) methods are some of the efficient thrust-vectoring techniques. Among the various FTVC methods, the use of the coanda effects downstream of the nozzle exit has drawn particular interests. Previous studies on the thrust vectoring technique have demonstrated that the utilizing the coanda effect downstream of the rectangular nozzle exit is able to deflect the jet direction to some extents.*

*In the present study, a test device measuring multi-component forces is used to reveal the characteristics of the thrust control technique when the coanda effect is applied in sonic jet flows. Detailed calibration and data analysis of the test device have confirmed a high level of accuracy for the present measurement system. Previous thrust-vectoring test results obtained for supersonic jet of Mach 2.0 showed that the over-expanded primary jet interferes with the coanda surface and thus deflected, even without activation of the co-flowing secondary jet, if the gap distance between the primary jet and the coanda surface is not separated far enough.*

*It has led us to consider a new simple control technique, such that the movement of a single coanda flap with no secondary flows can provide reasonable deflection angles without any extra consumption of control flows. The control method is applied to a sonic rectangular jet for various jet expansion conditions. Some static and dynamic characteristics of the control technique are presented in the paper.*

One previous study showed that Fluidic Thrust Vector Control (FTVC) methods can improve the thrust capacity per engine weight by 7-12% and the operating costs by 37-53% [1], with additional advantages in stealth operations and nozzle cooling benefits, as compared to the other conventional control methods. Of the various FTVC methods [2, 3], the one utilizing the coanda effect of the secondary flow injected at the nozzle exit has drawn particular interests. Some previous studies [4-6] demonstrated that those techniques work reasonable in deflecting the primary jet direction.

Those previous studies, however, have been restricted with respect to being able to control the thrust vector in relatively low-speeds and less compressible flow regimes [6-8]. A recent experimental [9] study regarding the supersonic 'co-flowing' FTVC technique also experienced limitations in revealing the quantitative performance-characteristics of the technique. A recent numerical study [10] on supersonic coanda flows also over-estimated the strength of the coanda effects.

In the present study, a test device using four load cells has been designed to accurately evaluate the characteristics of the thrust vectoring technique in supersonic regimes. Detailed calibration and data analysis of the test device have confirmed a high level of accuracy and precision for the present measurement system [11].

In the previous study regarding the application of co-flowing secondary flow for thrust vectoring of Mach 2.0 primary jet flows [12], the primary jet was observed to interfere with the coanda surface and thus to be deflected,

## 1 Introduction

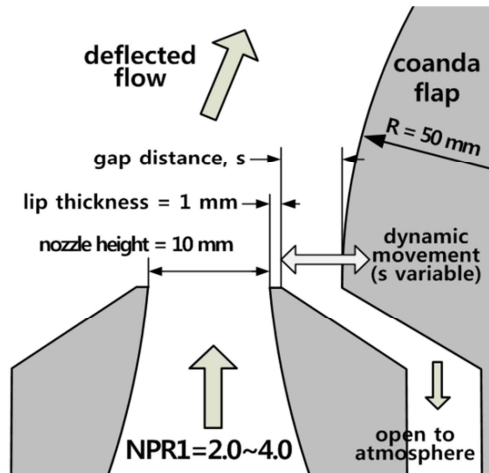


Fig. 1. Schematic of the nozzle and flap.

even without activation of the secondary jet. The observations have led us to consider a new simple control technique, such that it can introduce reasonable thrust vectoring by just a simple movement of the coanda flap with no secondary control flows. The control technique is applied to a sonic rectangular jet for various jet expansion conditions. Preliminary static and dynamic characteristics of the control technique are provided in the paper.

## 2 Experimental Setup

### 2.1 Rectangular nozzle and coanda flap

Figure 1 shows the configuration of the nozzle and the coanda flap utilized in the present study. The nozzle is designed as a converging nozzle, and thus the nozzle exit Mach number is 1.0. The nozzle exit height and width is 10 mm and 30 mm respectively. The coanda flap is located just beneath (right side in Fig. 1) the primary nozzle exit and spans the nozzle width. The nozzle assembly is designed for the coanda flap to be moved by a LM actuator and thus vary the gap distance ( $s$ ) between the nozzle exit and the flap surface. The gap distance can be varied continuously in the range of  $0 < s < 5$  mm. The radius of curvature ( $R$ ) of the coanda flap is fixed as 50 mm, however, the flap is changeable if needed, to cover wide range of test cases of  $s/R$  that is possibly one of critical parameters of the present thrust-vectoring performances.

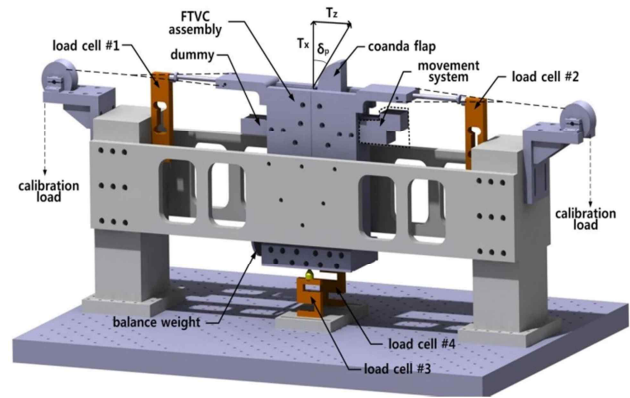


Fig. 2. Force measurement device with LM actuator to move the coanda flap.

### 2.2 Force measurement system

The schematic diagram of the test device is shown in Fig. 2. Signals from the four load cells (CAS) in the measurement device are digitally recorded by a bridge-circuit module (NI 9237, NI) at a 1 kHz sampling rate. The pivot points of the two load cells to measure the side thrusts are aligned to the nozzle exit, and two S-type load cells installed at the bottom center of the nozzle block measure the axial thrust. The nozzle chamber pressure is measured by using a pressure measurement scanner (PSI 9116, Measurements Specialities) at a 60 Hz sampling rate. Flow visualizations are also carried out by a Z-type schlieren setup using two schlieren mirrors and two optical mirrors. A short pulse light source (LS-201, KOMI) is synchronized to a CCD camera (CCE-B013-U, Mightex). The voltage signal of the load cells, signal from the actuator, the stagnation chamber pressure and digital flow visualization images are all synchronized and simultaneously saved on PC by the LabView. More detailed information including the calibration procedure and the measurement accuracy of the test device are presented in Reference 11.

### 2.2 Control of the flap movement

Figure 3 shows the detailed configuration of the nozzle assembly installed with the LM actuator. The actuator (SKR20) is designed to continuously move the flap by a stepping motor (A3K-S545) with a high accuracy. A dummy

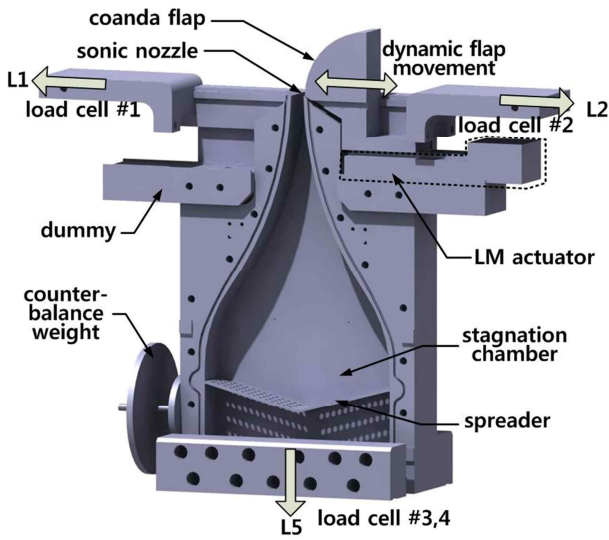


Fig. 3. Details of the nozzle and the actuator.

block is attached at the opposite side of the actuator to align the axis of center of gravity of the nozzle assembly to the load cell installed at the bottom (#3, #4 in Fig. 3), and an additional counter-balance weight is attached to the side of the nozzle block for a fine-tuning of the center of gravity of the nozzle assembly, and thus the tare loads transmitted to the side load cells are eliminated.

### 3 Results and Discussion

#### 3.1 Flow interferences with the coanda flap

Schlieren flow visualizations for various gap distances ( $s$ ) obtained in the previous study [12] are shown in Fig. 4. In the study, FTVC technique was applied to the supersonic rectangular jet of Mach 2.0, with co-flowing

secondary control flows of various pressures ( $P_{i2}$ ). In the figure, the secondary jet is not activated for all three cases and only  $s$  is varied. The total pressure of the primary jet ( $P_{t1}$ ) is fixed as  $300 \text{ kPa}$  ( $NPR1 = 3.0$ ) for all the cases. Here  $NPR1$  is defined as the ratio of the total pressure of the primary jet to the ambient pressure. The resultant pitch deflection angle ( $\delta_p$ ) directly measured by the load cells is also depicted in each image in the figure. Here the deflection angle is defined as  $\tan^{-1}(T_z/T_x)$ , where  $T_x$ ,  $T_z$  are the axial thrust and the side thrust, respectively.

In Fig. 4a, the gap distance is close to the nozzle exit lip ( $s = 1.0 \text{ mm}$ ). Although the secondary jet is not activated, it is apparent that the primary jet is substantially deflected toward the flap surface (the right direction in the figure). In Fig. 4c, it is noticed that the primary jet is straight and there is no interference with the downstream coanda flap surface. The reason of those interference phenomena is presumed that, if the gap distance is small enough, the nozzle exit just above the coanda surface could act like a back step [13,14], and that a recirculating flow just beneath the nozzle exit is thought to form a confinement between the primary jet and the flap surface.

Flow phenomena due to those back-step effects with no flow control are quantitatively depicted in Fig. 5 [15]. Regression curves assuming a linear variation of the deflection angle are also shown in the figure. In Fig. 5, it is noticed that the deflection angle almost linearly decreases as  $s$  increases up to near  $4 \text{ mm}$ . It is interesting to notice that the slopes of those variations are similar irrespective of  $NPR1$ .

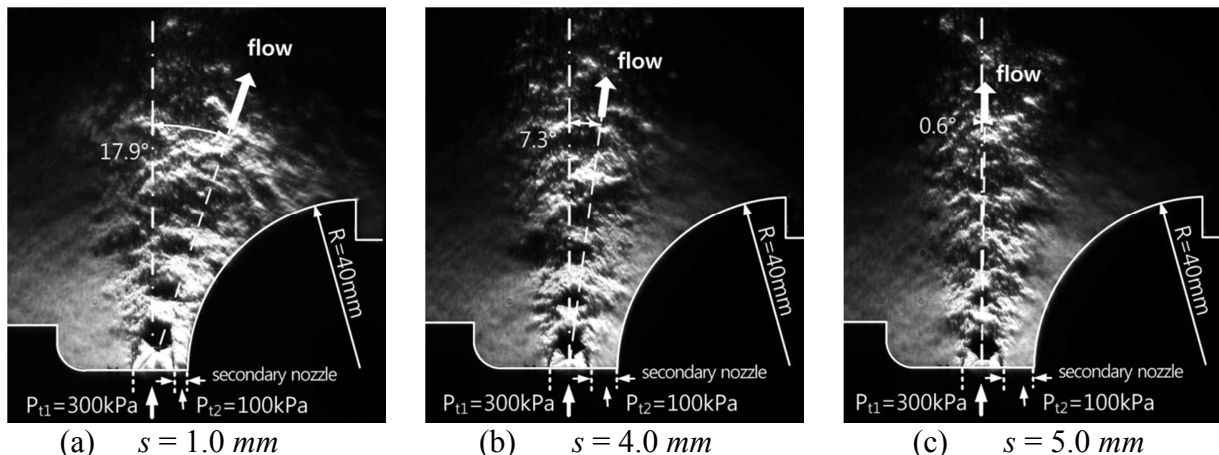


Fig. 4. Schlieren visualizations without activation of the coanda jet ( $P_{t1} = 300 \text{ kPa}$ ,  $P_{i2} = 100 \text{ kPa}$ ).

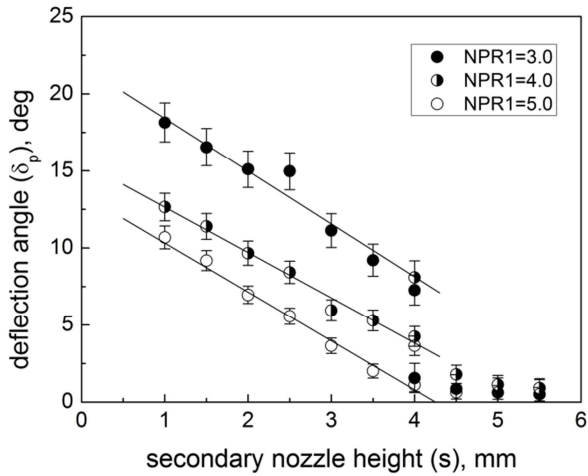


Fig. 5. Deflection angles without control flow [15].

When  $s$  becomes slightly larger than 4 mm, it is observed that the primary jet begins to show sudden unstable fluctuations, again irrespective of the value of  $NPR1$  (or  $P_{t1}$ ). As the gap ( $s$ ) is further increased, the strong unsteadiness fades away and the back step effect becomes almost negligible when  $s$  reaches to 5.0 mm.

### 3.2 Thrust vectoring for the sonic nozzle

Schlieren flow visualizations obtained for the present sonic nozzle for various gap distances are shown in Fig. 6. The total pressure of the jet is fixed as 300 kPa ( $NPR1 = 3.0$ ) to compare with the images shown in Fig. 4. In Fig. 6a, the gap distance is set to 0 (note the lip thickness of the nozzle exit,  $t$ , is 1 mm). It is apparent that the sonic jet is deflected toward the flap surface, and a strong oblique shock at the nozzle exit is formed over the flap surface.

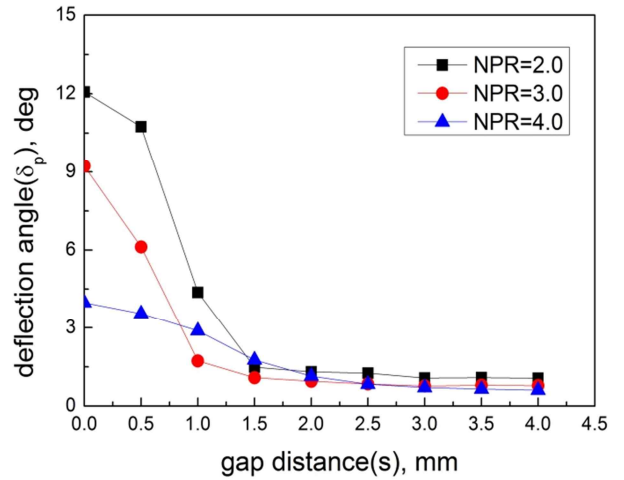


Fig. 7. Deflection angles for various  $NPR1$ .

A slight movement of the flap introduces a substantial change in shock structures in the flow field. As shown in Fig. 6c, the previous strong coanda effect associated with the oblique shock at the nozzle exit is diminished by the slight flap relocation ( $s = 1.0$  mm).

Variations of the deflection angle ( $\delta_p$ ) measured for the sonic nozzle are shown in Fig. 7 for various  $NPR1$ s. In Fig. 7, it is observed that the deflection angle decreases as  $s$  increases, regardless of the nozzle pressures. The higher the nozzle pressure is, the smaller the deflection angle normally becomes for the same gap distance. When the gap distance is larger than 1 mm, the coanda effects are almost negligible, irrespective of  $NPR1$ . It is obvious that the strength of the jet expansion is one of the essential parameters in the present thrust vectoring control, and that it is more efficient for smaller value of  $NPR1$  in such high-speed flow regimes. In the figure, it is also observed

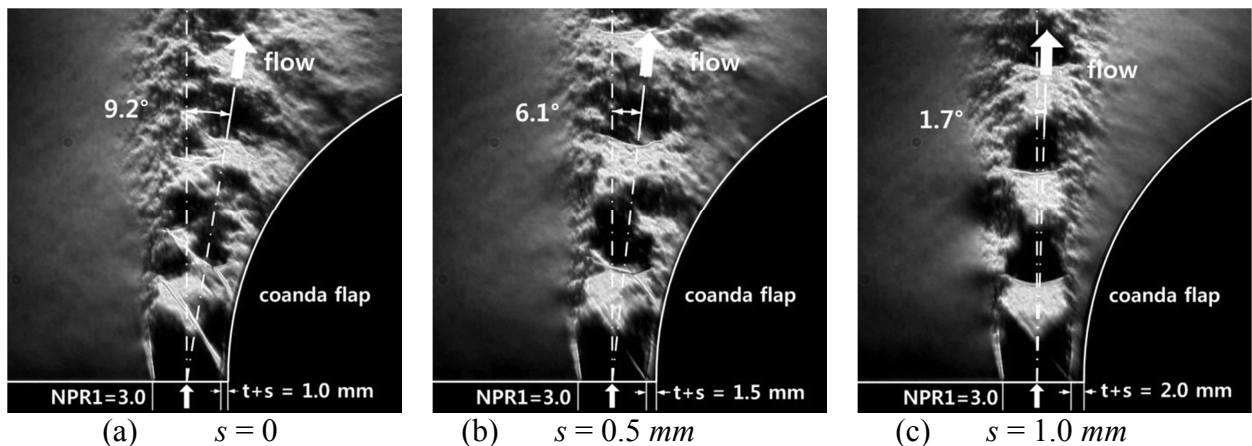


Fig. 6. Schlieren visualizations for the sonic nozzle for various  $s$  ( $NPR1 = 3.0$ ).

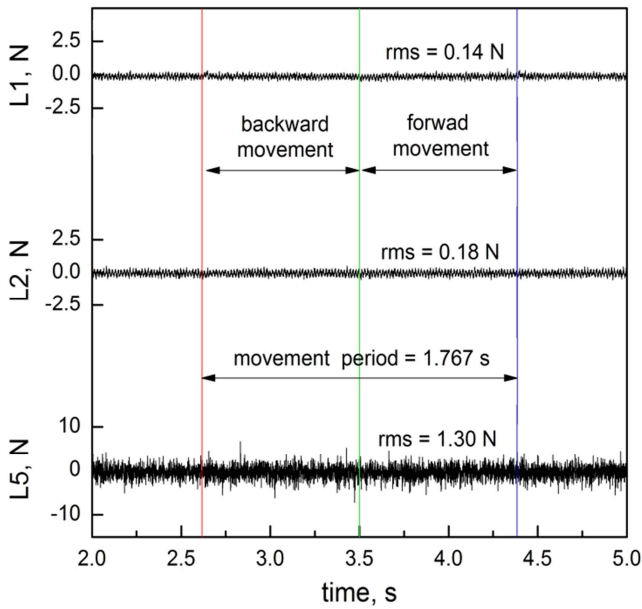


Fig. 8. Load cell signals during the flap stroke.

the deflection angles for the sonic nozzle are smaller than those observed in the previous study (Mach 2.0, see Fig. 5) for the same gap distance and  $NPR_1$ .

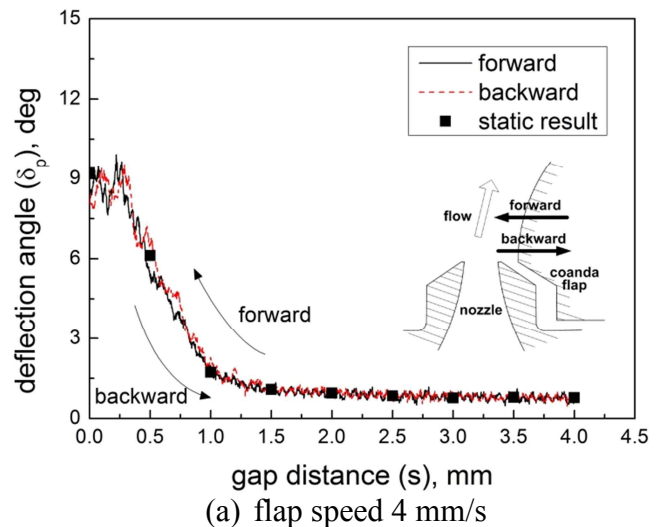
### 3.3 Flow behaviors during flap movements

Effects of the coanda flap movement itself to the load cell signal are observed before preceding the dynamic tests. Flap movement during tests could introduce a shift of the center of gravity of the nozzle assembly and unwanted torques in the force measurement system. Figure 8 shows timewise variation of the load cell signals during the flap movement with no sonic jet activated. The stroke (round-trip) distance of the flap is set to 7 mm, and the flap speed is 8 mm/s.

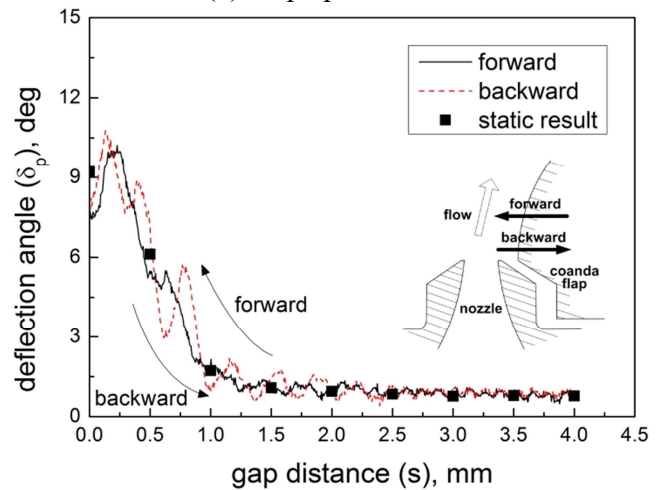
As shown in the figure, it is obvious that the characteristics of the noise signals from the load cells are not influenced at all by the flap movement. The  $rms$  values of the load cell signals measuring the side thrusts ( $L1$  and  $L2$  in Fig. 8, also see Fig. 3) are in the ranges between 0.14 N to 0.18 N. Since typical measurement ranges of the side thrusts are up to 10 N, the present signal to noise ratio is acceptable, except the cases of very low side thrusts. The  $rms$  value of the load cell signal measuring the axial thrust ( $L5$  in Fig. 8, also see Fig. 3) is about 1.30 N. Again, considering the typical

measurement values of the load cell  $L5$  ranges from 150 N to 200 N (including the weight of the nozzle assembly itself), the signal to noise ratio of the load cell is also satisfactory. Similar observations are also carried out for a different flap speed (4 mm/s), and it is found that the noise characteristics are not influenced by the flap speed.

To get a general understanding of the dynamic behaviors of the thrusting jet flow during the flap movement, Fig. 9 shows the dynamic variation of the deflection angle versus the gap distance for various flap speeds and  $NPR_1$ s. Figure 9a shows the case of the flap speed equal to 4 mm/s, and Fig. 9b shows the case of flap speed equal to 8 mm/s. The nozzle pressure is set to 300 kPa, and both the stroke distance is the same as 4 mm.



(a) flap speed 4 mm/s



(b) flap speed 8 mm/s

Fig. 9. Dynamic characteristics of the deflection angle ( $NPR_1 = 3.0$ ).

In the figure, the solid symbols represent the deflection angles obtained in the ‘static’ tests, and the lines represent the angles observed in the ‘dynamic’ tests. It is found that there is no appreciable difference between the static and the dynamic deflection angles, *i.e.*, the dynamic data closely match with the results of the static tests over the full ranges of  $s$ , except for the case of  $s$  equal to zero at flap speed of  $8 \text{ mm/s}$ . As shown in the figure, some unsteady effects are evident. Especially, weak fluctuations in the range of  $1 \text{ mm} < s < 4 \text{ mm}$  get stronger as the flap speed increases. At the present, those fluctuations are presumed to be somewhat associated with room noises (dominant frequency near  $60 \text{ Hz}$ ), since the measured side thrusts in the range are weak and easily influenced by the noises.

To reveal any hysteresis characteristics of the thrusting during the stroke of the flap, the solid line depicts the variation of the deflection angle when the flap gets closer (forward) to the nozzle exit lip, and the dotted line depicts for the flap retraction (backward) case in the figure. In Fig. 9a (flap speed =  $4 \text{ mm/s}$ ), not much difference are observed in the variation of the deflection angles during the stroke.

However, it is interesting to note that appreciable variations, *i.e.*, hysteresis effects, in the behavior of the deflection angle exhibits during the stroke, if the flap speed gets faster to  $8 \text{ mm/s}$  (see Fig 9b). Relatively strong periodic fluctuations of a low-frequency (near  $20 \text{ Hz}$ ) in the thrusting jet flow are present in Fig 9b, especially when the flap is retracted from the nozzle exit ( $0 < s < 1 \text{ mm}$ ). Detailed observations of the nozzle chamber pressure, the axial thrust and the side thrust during the dynamic tests reveals that those low-frequency fluctuations of the deflection angle are mostly influenced by the fluctuating side thrust itself. Despite detailed results are not shown in the present paper, those phenomena of low-frequency fluctuation of the thrusting jet flow during the flap movement get stronger if the nozzle pressure increases.

## 4 Conclusions

Static and dynamic characteristics of the control technique utilizing the coanda effect in a sonic rectangular jet have been experimentally studied, and the conclusions are as follows:

1) It is observed that the deflection angle decreases as the gap distance between the nozzle exit and the flap surface becomes larger, regardless of the primary nozzle pressures. The higher the nozzle pressure is, the smaller the deflection angle becomes for the same gap distance. In such highly compressible flow regimes, the present control technique becomes less efficient as the jet expansion gets stronger.

2) When the gap distance is larger than  $1 \text{ mm}$ , the coanda effects are essentially negligible, irrespective of the nozzle pressures. It is also observed all the deflection angles for the sonic nozzle are smaller for the same gap distances and nozzle pressures, as compared to the previous observations in Mach 2.0 nozzle.

3) For the relatively low flap speed, not much difference is observed in the variation of the deflection angles during the flap stroke. However, a strong hysteresis behavior of the deflection angle exhibits during the flap stroke for higher flap speed. Periodic fluctuations of a low-frequency near  $20 \text{ Hz}$  are also observed in the thrusting jet flow, especially when the flap is retracted from the nozzle.

## Acknowledgments

This research was supported by the Basic Science Research Program through the National Research Foundation of Korea (NRF) funded by the Ministry of Education, Science and Technology (2012R1A1A2006348).

## References

- [1] Deere, K. A., “Summary of Fluidic Thrust Vectoring Research Conducted at NASA Langley Research Center,” AIAA Paper 2003-3800, 2003.
- [2] Wing, D. J., “Static Investigation of Two Fluidic Thrust-Vectoring Concepts on a Two-Dimensional Convergent Divergent Nozzle,” *NASA Technical Memorandum 4574*, 1994.
- [3] Strykowski, P. J., Krothapalli, A., and Forliti, D. J., “Counterflow Thrust Vectoring of Supersonic Jets,” *AIAA Journal*, Vol. 34, No. 11, pp. 2306-2314, 1996.

- [4] Flamm, J. D., Deere, K. A., Mason, M. L., Berrier, B. L., and Johnson, S. K., "Design Enhancements of the Two-Dimensional, Dual Throat Fluidic Thrust Vectoring Nozzle Concept," AIAA Paper 2006-3701, 2006.
- [5] Neely, A. J., Gesto, F. N., Young J., "Performance Studies of Shock Vector Control Fluidic Thrust Vectoring," AIAA Paper 2007-5086, 2007.
- [6] Mason, M. S., Crowther, W. J., "Fluidic Thrust Vectoring for Low Observable Air Vehicle," AIAA Paper 2004-2210, 2004.
- [7] Banazadeh, A., Saghafi, F., Ghoreyshi, M., Pilidis, P., "Experimental and Computational Investigation into the Use of Co-flow Fluidic Thrust Vectoring on a Small Gas Turbine," *The Aeroautical Journal*, Vol. 112, No. 1127, pp.17-25, 2008.
- [8] Crowther, W. J., Wilde, P. I. A., Gill, K., Michie, S. M., "Towards Integrated Design of Fluidic Flight Controls for a Flapless Aircraft," *The Aeroautical Journal*, Vol. 113, No. 1149, pp.699-713, 2009.
- [9] Yoon, S. H., Jun, D. H., Heo, J. Y., Sung, H. G., Lee, Y., "Experimental Study of Thrust Vectoring of Supersonic Jet Using Co-flowing Coanda Effects," *Journal of The Korean Society Aeronautical and Space Sciences*, Vol. 40, No. 11, pp. 927-933, 2012.
- [10] Gross, A., and Fasel, H. F., "Coanda Wall Jet Calculations Using One- and Two-Equation Turbulence Models," *AIAA Journal*, Vol. 44, No. 9, pp. 2095-2107, 2006.
- [11] Song, M. J., Chang, H. B., Cho, Y. H., Lee, Y., "Development of the High-Accuracy Multi-Component Balance for Fluidic Thrust Vectoring Nozzle of UAV," *J. of the Korean Society for Aeronautical and Space Sciences*, Vol. 41, No. 2, pp. 142-149, 2013.
- [12] Song, M. J., Park, S. H., Chang, H. B., Cho, Y. H., and Lee, Y., "Application of Back-Step Coanda Flap for the Supersonic Co-flowing Fluidic Thrust Vector Control," AIAA 2013-3951, 49<sup>th</sup> AIAA/ASME/SAE/ASEE Joint Propulsion Conference, July 2013.
- [13] Gregory-Smith, D. G., Senior, P., "The Effects of Base Steps and Axisymmetry on Supersonic Jets over Coanda Surfaces," *Int. J. Heat and Fluid Flow*, Vol. 15, No. 4, pp.291-298, 1994.
- [14] Carpenter, P. W., Smith, C., "The Aeroacoustics and Aerodynamics of High-Speed Coanda Devices, Part 2: Effects of Modifications for Flow Control and Noise Reduction," *Journal of Sound and Vibration*, Vol. 208, No. 5, pp. 803-822, 1997.
- [15] Song, M. J., Park, S. H., and Lee, Y., "Application of Back-Step Coanda Flap for Supersonic Co-flowing Fluidic Thrust Vector Control," accepted for publication, *AIAA Journal*, May 2014.

### **Copyright Statement**

The authors confirm that they, and/or their company or organization, hold copyright on all of the original material included in this paper. The authors also confirm that they have obtained permission, from the copyright holder of any third party material included in this paper, to publish it as part of their paper. The authors confirm that they give permission, or have obtained permission from the copyright holder of this paper, for the publication and distribution of this paper as part of the ICAS 2014 proceedings or as individual off-prints from the proceedings.

### **Contact Author Email Address**

mailto:ylee@kau.ac.kr